TDOA Data Selection for Accurate Passive Coherent Location

Daniel P. Nicolalde-Rodríguez, *Student Member, IEEE,* Wallace A. Martins, *Senior Member, IEEE,*
José A. Apolinário Jr., *Senior Member, IEEE,* and Marcello L. R. de Campos, *Senior Member, IEEE.*

Abstract—This paper addresses the problem of selecting suitable time difference of arrival (TDOA) measurements for passive coherent location with multiple–transmitters/receivers. Firstly, we propose a unified mathematical framework for the following target location algorithms: spherical interpolation (SI), spherical intersection (SX), and nonlinearly constrained least squares (NLCLS). This paper generalizes the currently available models for scenarios with multiple–transmitters/one–receiver and one–transmitter/multiple–receivers. The SI/SX algorithms use closed-form expressions to tackle the location problem without considering all the nonlinear relationships among the optimization variables. As for the NLCLS algorithm, such nonlinearities are taken into account with the help of nonlinear constraints. Effects like multipath propagation and shadow fading increase TDOA measurement values resulting in outliers. To remove the outliers, we propose three TDOA selection processes. The first one uses a simple comparison rule. The second approach iteratively detects outliers based on cost function comparisons. The last approach divides the search region into cuboids. The cuboid-based approach separates consistent TDOAs from outliers, and its centroid represents a new location estimate. The numerical experiments show that the proposed cuboid-based method has greater robustness when increasing the probability of outliers.

Index Terms—Passive coherent location, time difference of arrival, TDOA selection, outliers, cuboid.

I. INTRODUCTION

PASSIVE coherent location (PCL) systems have been used for they do not need exclusive transmitters (TXs) to detect and locate target units [1], [2]. PCL systems, also known as passive radars, use already deployed electromagnetic radio systems like analog audio broadcaster (FM), digital audio broadcasting (DAB), digital video broadcaster-terrestrial (DVB-T), automatic identification system satellite (AIS-S), global positioning system (GPS), and mobile communication systems (2G, 3G, 4G, and 5G) [3]. In these systems TXs are illuminators of opportunity that cover the location region.

Many different PCL investigations have been conducted based on time difference of arrival (TDOA) measurements [4]–[11]. TDOA represents the time difference between the signal emitted by the TX and collected by the RX (Reference channel) and the replicated signal reflected in the target (Surveillance channel). The literature mainly deals with TDOA–based

D. P. Nicolalde-Rodríguez and M. L. R. de Campos are with the Electrical Engineering Program (PEE), COPPE / Federal University of Rio de Janeiro (UFRJ), Rio de Janeiro, RJ, Brazil (e-mails: danielnicolalde@gmail.com; campos@smt.ufrj.br). W. A. Martins is with the Interdisciplinary Centre for Security Reliability and Trust (SnT), University of Luxembourg (UniLu), Luxembourg (e-mail: wallace.alvesmartins@uni.lu). J. A. Apolinário, Jr. is with the Department of Electrical Engineering, Military Institute of Engineering (IME), Rio de Janeiro, RJ, Brazil (e-mail: apolin@ime.eb.br).

PCL solutions either for multiple TXs and one RX, or for multiple RXs and one TX. However, the authors in [12] present a least square solution of a passive location system based on time sum of arrival (TSOA) measurements in a scenario of multiple TXs and multiple RXs. TSOA represents the travel time of the signal reflected in the target and associated with a specific TX-RX pair. Nevertheless, a PCL formulation consisting of TDOA measurements associated with multiple TXs and RXs is also possible. Current systems as 5G NR (New Radio) technology, with massive multiple–input and multiple–output (MIMO) and flexible frequency access, expect to use a dynamic location scenario that takes advantage of multiple TXs and RXs with low latency and high reliability [13]–[15].

This paper extends the formulation of PCL algorithms using spherical intersection (SX) and spherical interpolation (SI), previously derived for multiple TXs and one RX scenario [7] as well as multiple RXs and one TX scenario [8], to the general case of multiple TXs and multiple RXs. We also propose the multiple TXs and multiple RXs formulation of the nonlinearly constrained least square (NLCLS) algorithm, designed initially for multiple RXs and one TX [8], where we use all the constraints to improve the accuracy of the original SI technique. In addition, the paper proposes a simplified scheme (S-NLCLS) with a single constraint. In terms of accuracy, S-NLCLS is close to NLCLS, but with reduced computational load.

Location algorithms usually rely on accurate TDOA estimation for each TX-RX pair. It is common, however, that among the TDOA measurements we find outliers. An outlier has a much larger value than a nominal TDOA, and it may appear due to effects such as multipath propagation and shadow fading [16]. For example, multipath propagation generally produces outliers considering that the generated propagation signal has a longer path than the signal reflected in the target. Moreover, the shadow fading effect can introduce a high attenuation due to the large-scale fluctuation (line-of-sight blocking), therefore creating a longer signal path [17].

In order to improve the performance of PCL algorithms, one may appropriately select TDOA measurements (removing outliers). Investigations for selecting time difference of flight (TDOF) and time of flight (TOF) measurements have been published for active location systems (when the target directly receives reference signals from transmitters or when the target emits reference signals that sensors detect) [17]–[24].

The authors in [20] and [21] proposed region-based search algorithms that select consistent TOF/TDOF measurements for acoustic sensor location. The proposals split the location

region into cuboids. The cuboid that potentially contains the target location separates consistent data from outliers. This cuboid is associated with most TOF/TDOF measurements. Considering that a region of constant TDOF is a hyperboloid of two sheets with foci located at two loudspeakers, the problem could be seen as selecting the cuboid that intersects most of the hyperboloids associated with the different pairs of loudspeakers. We extend this criterion to PCL, where the selected cuboid intersects most of the ellipsoids associated with most TDOA measurements collected from the different TX/RX pairs. Moreover, the centroid of the final cuboid that separates consistent TDOAs and outliers can be considered a new target estimate. As will be seen in Section V, this proposed target location estimation shows promising results in terms of accuracy, especially when reducing the cuboid sizes.

Other techniques select data based on comparisons of cost-function evaluations over different combinations of TDOA data. The works in [19] and [12] select, respectively, TDOAs in a source location system and TSOAs in a passive location system. They define a fixed number of selected data, and the data set that obtains the least cost is employed to compute the final location. On the other hand, an iterative procedure in [25], [26] removes, one-by-one, time delay estimates (TDEs) associated with a pair of acoustic sensors in a scenario that detects direction of arrival of gunshots. The algorithm's stopping criterion also depends on a fixed number of selected data. We proposed another TDOA selection method for PCL that iteratively discards outliers (one-by-one) of a candidate list. At each iteration, a cost function determines the TDOA measurement that must be discarded. The iterative process stops automatically when all the selected TDOA errors are below a predefined threshold. We also benchmark our proposal against a simple TDOA selection technique that quickly removes outliers using a simple decision ratio.

The organization of this paper is as follows. Section II describes the mathematical formulation of PCL algorithms (SI, SX, and NLCLS/S-NLCLS) in the scenario of multiple TXs and multiple RXs. Section III addresses the proposed selection methods that separate consistent TDOA measurements from outliers. Section IV details the adaptation that must be carried out in the location algorithm, the removal of columns and rows of the matrices and vectors associated with outliers previously selected. Section V presents the experimental results obtained from simulations. Finally, conclusions are stated in Section VI.

II. LOCALIZATION ALGORITHMS

We assume M RXs and L TXs denoted as RXm, $m \in \mathcal{M} \triangleq \{1, 2, \ldots, M\}$, and TX$l$, $l \in \mathcal{L} \triangleq \{1, 2, \ldots, L\}$, respectively. Fig. 1 sketches the PCL geometry of the pair RXm-TXl. Vectors $\mathbf{p}_{\text{RX}m}$ and $\mathbf{p}_{\text{TX}l}$ represent the known positions of RXm and TXl, respectively. The unknown location of the target is represented by vector $\mathbf{p}_{\text{T}}$. The target location system can be applied for an N–dimension problem, $N \in \{2, 3\}$.

As shown in Fig. 1, the distances of interest in the PCL scenario are defined as: TXl–target distance $r_{\text{TX}l\text{-T}} \triangleq \|\mathbf{p}_{\text{TX}l} - \mathbf{p}_{\text{T}}\|$, RX$m$–target distance $r_{\text{RX}m\text{-T}} \triangleq \|\mathbf{p}_{\text{RX}m} - \mathbf{p}_{\text{T}}\|$, and RX$m$–TX$l$ distance $r_{\text{RX}m\text{-TX}l} \triangleq \|\mathbf{p}_{\text{RX}m} - \mathbf{p}_{\text{TX}l}\|$.
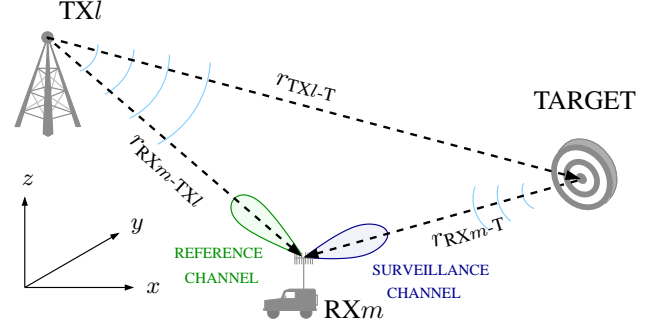

Fig. 1. Geometry of a passive coherent location system.

In PCL jargon, the difference between the reflected path length ($r_{\text{RX}m\text{-T}} + r_{\text{TX}l\text{-T}}$) and the line-of-sigh length ($r_{\text{RX}m\text{-TX}l}$) is known as bistatic range [1]. For each pair RXm–TXl, we denote its bistatic range as

$$r_{\text{B}ml} \triangleq r_{\text{RX}m\text{-T}} + r_{\text{TX}l\text{-T}} - r_{\text{RX}m\text{-TX}l}. \tag{1}$$

The range difference (reflected path length) of the RXm–TXl pair, r_{ml}, is the total distance defined by the bistatic range plus the line-of-sight distance, $r_{\text{B}ml} + r_{\text{RX}m\text{-TX}l}$, which from Eq. (1) becomes

$$r_{ml} = r_{\text{RX}m\text{-T}} + r_{\text{TX}l\text{-T}}, \tag{2}$$

which is the basis of the PCL approach for multiple TXs/RXs.

From Eq. (2), we have an identity that, after squaring, yields

$$\left(r_{ml} - r_{\text{TX}l\text{-T}}\right)^2 = r_{\text{RX}m\text{-T}}^2, \tag{3}$$

Eq. (3) is the second degree equation used to formulate the PCL problem when the number of RXs is larger than the number of TXs, i.e., when $M \geq L$. In case $L \geq M$, one can use

$$\left(r_{ml} - r_{\text{RX}m\text{-T}}\right)^2 = r_{\text{TX}l\text{-T}}^2. \tag{4}$$

In this paper, we assume $M \geq L$ in the forthcoming derivations for the sake of conciseness.

Eq. (3) can be rewritten as

$$\bar{\mathbf{p}}_{\text{RX}m\text{-TX}l}^{\mathsf{T}} \bar{\mathbf{p}}_{\text{T-TX}l} - r_{ml} r_{\text{TX}l\text{-T}} = \frac{1}{2}(r_{\text{RX}m\text{-TX}l}^2 - r_{ml}^2), \tag{5}$$

where $\bar{\mathbf{p}}_{\text{RX}m\text{-TX}l} \triangleq \mathbf{p}_{\text{RX}m} - \mathbf{p}_{\text{TX}l}$ and $\bar{\mathbf{p}}_{\text{T-TX}l} \triangleq \mathbf{p}_{\text{T}} - \mathbf{p}_{\text{TX}l}$. The unknown variables $\bar{\mathbf{p}}_{\text{T-TX}l}$ and $r_{\text{TX}l\text{-T}}$ must be computed to find the estimated target location.

To consider the complete data in our PCL scenario (M RXs, L TXs, and one target), we define the $ML \times NL$ matrix $\mathbf{P}_{\text{RX-TX}}$ as

$$\mathbf{P}_{\text{RX-TX}} \triangleq \begin{bmatrix} \bar{\mathbf{P}}_{\text{RX-TX}1} & \cdots & \mathbf{0}_{M \times N} & \cdots & \mathbf{0}_{M \times N} \\ \vdots & \ddots & \vdots & \ddots & \vdots \\ \mathbf{0}_{M \times N} & \cdots & \bar{\mathbf{P}}_{\text{RX-TX}l} & \cdots & \mathbf{0}_{M \times N} \\ \vdots & \ddots & \vdots & \ddots & \vdots \\ \mathbf{0}_{M \times N} & \cdots & \mathbf{0}_{M \times N} & \cdots & \bar{\mathbf{P}}_{\text{RX-TX}L} \end{bmatrix}, \tag{6}$$

where the $M \times N$ matrix $\bar{\mathbf{P}}_{\text{RX-TX}l}$ is given as

$$\bar{\mathbf{P}}_{\text{RX-TX}l} \triangleq \begin{bmatrix} \bar{\mathbf{p}}_{\text{RX1-TX}l}^{\mathsf{T}} \\ \vdots \\ \bar{\mathbf{p}}_{\text{RX}M\text{-TX}l}^{\mathsf{T}} \end{bmatrix}. \tag{7}$$

We also define the $ML \times L$ matrix $\mathbf{R}$ as

$$\mathbf{R} \triangleq \begin{bmatrix} \mathbf{r}_1 & \ldots & \mathbf{0}_{M\times 1} & \ldots & \mathbf{0}_{M\times 1} \\ \vdots & \ddots & \vdots & \ddots & \vdots \\ \mathbf{0}_{M\times 1} & \ldots & \mathbf{r}_l & \ldots & \mathbf{0}_{M\times 1} \\ \vdots & \ddots & \vdots & \ddots & \vdots \\ \mathbf{0}_{M\times 1} & \ldots & \mathbf{0}_{M\times 1} & \ldots & \mathbf{r}_L \end{bmatrix}, \qquad (8)$$

where $\mathbf{r}_l \triangleq \begin{bmatrix} r_{1l} & \ldots & r_{ml} & \ldots & r_{Ml} \end{bmatrix}^\mathsf{T}$. Moreover, $\bar{\mathbf{p}}_{\text{T-TX}}$ ($NL \times 1$ vector), $\mathbf{r}_{\text{TX-T}}$ ($L \times 1$ vector), and $\mathbf{z}$ ($ML \times 1$ vector) are defined as

$$\bar{\mathbf{p}}_{\text{T-TX}} \triangleq \begin{bmatrix} \bar{\mathbf{p}}_{\text{T-TX1}} \\ \vdots \\ \bar{\mathbf{p}}_{\text{T-TXL}} \end{bmatrix}, \mathbf{r}_{\text{TX-T}} \triangleq \begin{bmatrix} r_{\text{TX1-T}} \\ \vdots \\ r_{\text{TXL-T}} \end{bmatrix}, \mathbf{z} \triangleq \begin{bmatrix} \mathbf{z}_1 \\ \vdots \\ \mathbf{z}_L \end{bmatrix}, \qquad (9)$$

where $\mathbf{z}_l$ ($M \times 1$ vector) has the following structure:

$$\mathbf{z}_l \triangleq \frac{1}{2} \begin{bmatrix} r_{\text{RX1-TX}l}^2 - r_{1l}^2 \\ \vdots \\ r_{\text{RXM-TX}l}^2 - r_{Ml}^2 \end{bmatrix} = \begin{bmatrix} z_{1l} \\ \vdots \\ z_{Ml} \end{bmatrix}. \qquad (10)$$

Considering Eq. (5) applied for M RXs and L TXs, we have

$$\mathbf{P}_{\text{RX-TX}} \bar{\mathbf{p}}_{\text{T-TX}} - \mathbf{R} \mathbf{r}_{\text{TX-T}} = \mathbf{z}. \qquad (11)$$

Associating matrix $\mathbf{A} \triangleq \begin{bmatrix} \mathbf{P}_{\text{RX-TX}} & -\mathbf{R} \end{bmatrix}$ with known variables, Eq. (11) can be expressed as

$$\mathbf{A} \underbrace{\begin{bmatrix} \bar{\mathbf{p}}_{\text{T-TX}} \\ \mathbf{r}_{\text{TX-T}} \end{bmatrix}}_{\triangleq \mathbf{x}} = \mathbf{z}. \qquad (12)$$

The entries of $\mathbf{x}$ are nonlinearly related since $\mathbf{r}_{\text{TX-T}}$ is a (known) nonlinear function of $\bar{\mathbf{p}}_{\text{T-TX}}$, which makes Eq. (12) a nonlinear equation on $\bar{\mathbf{p}}_{\text{T-TX}}$. Moreover, Eq. (12) does not usually hold equality when we employ practical measurements to obtain the target location, so that usually one searches for $\bar{\mathbf{p}}_{\text{T-TX}}$ that minimizes some model mismatch metric (e.g., a norm of the error vector $\mathbf{e} \triangleq \mathbf{A}\mathbf{x} - \mathbf{z}$).

Following [7], two classical methods approximate the solution $\bar{\mathbf{p}}_{\text{T-TX}}$ to the nonlinear Eq. (12), namely: spherical interpolation (SI) and spherical intersection (SX). The application of the two methods to the case of multiple TXs and one RX is addressed in [7], and to the scenario of multiple RXs and one TX is addressed in [8]. In the following, we extend the mathematical formulations of the two methods to the more generic case of multiple TXs and multiple RXs.

A. Spherical Interpolation

Eq. (12) can be approached using the unconstrained least square (LS) solution, which is obtained by equating to the null vector the gradient of the LS cost function $\xi(\mathbf{x})$, i.e., $\nabla_{\mathbf{x}} \xi(\mathbf{x}) = \mathbf{0}$, where

$$\xi(\mathbf{x}) \triangleq \mathbf{e}^\mathsf{T} \mathbf{e}. \qquad (13)$$

Thus, knowing that $\mathbf{A}$ is $ML \times (N+1)L$, a necessary condition for $\mathbf{A}^\mathsf{T}\mathbf{A}$ to be invertible is $M \geq N+1$, i.e., the number of receivers must be larger than the problem dimension (2D or 3D); in that case, the unconstrained LS solution becomes

$$\hat{\mathbf{x}} = (\mathbf{A}^\mathsf{T} \mathbf{A})^{-1} \mathbf{A}^\mathsf{T} \mathbf{z} = \begin{bmatrix} \hat{\bar{\mathbf{p}}}_{\text{T-TX}} \\ \hat{\mathbf{r}}_{\text{TX-T}} \end{bmatrix}. \qquad (14)$$

Note that $\hat{\bar{\mathbf{p}}}_{\text{T-TX}}$ corresponds to the first NL elements of $\hat{\mathbf{x}}$. Since we can express $\bar{\mathbf{p}}_{\text{T-TX}}$ as

$$\underbrace{\begin{bmatrix} \mathbf{p}_{\text{T}} - \mathbf{p}_{\text{TX1}} \\ \vdots \\ \mathbf{p}_{\text{T}} - \mathbf{p}_{\text{TXL}} \end{bmatrix}}_{\bar{\mathbf{p}}_{\text{T-TX}}} = \underbrace{\begin{bmatrix} \mathbf{I}_{N\times N} \\ \vdots \\ \mathbf{I}_{N\times N} \end{bmatrix}}_{\mathbf{I}_{\text{a}}} \mathbf{p}_{\text{T}} - \underbrace{\begin{bmatrix} \mathbf{p}_{\text{TX1}} \\ \vdots \\ \mathbf{p}_{\text{TXL}} \end{bmatrix}}_{\mathbf{p}_{\text{TX}}}, \qquad (15)$$

we expect to have $\hat{\bar{\mathbf{p}}}_{\text{T-TX}} \approx \mathbf{I}_{\text{a}} \mathbf{p}_{\text{T}} - \mathbf{p}_{\text{TX}}$, and therefore the final estimate of $\mathbf{p}_{\text{T}}$ is computed as

$$\hat{\mathbf{p}}_{\text{T}} = (\mathbf{I}_{\text{a}}{}^\mathsf{T} \mathbf{I}_{\text{a}})^{-1} \mathbf{I}_{\text{a}}{}^\mathsf{T} \left(\hat{\bar{\mathbf{p}}}_{\text{T-TX}} + \mathbf{p}_{\text{TX}} \right), \qquad (16)$$

which represents the mean of L individual estimates for each case of 1 TX and M RXs:

$$\hat{\mathbf{p}}_{\text{T}} = \frac{1}{L} \sum_{l=1}^{L} \left(\hat{\bar{\mathbf{p}}}_{\text{T-TX}l} + \mathbf{p}_{\text{TX}l} \right). \qquad (17)$$

B. Spherical Intersection

From Eq. (11), we can estimate $\bar{\mathbf{p}}_{\text{T-TX}}$ as

$$\hat{\bar{\mathbf{p}}}_{\text{T-TX}} = \mathbf{P}^\dagger \left(\mathbf{z} + \mathbf{R} \mathbf{r}_{\text{TX-T}} \right), \qquad (18)$$

where $\mathbf{P}^\dagger = (\mathbf{P}_{\text{RX-TX}}^\mathsf{T} \mathbf{P}_{\text{RX-TX}})^{-1} \mathbf{P}_{\text{RX-TX}}^\mathsf{T}$ and, in this case, a necessary condition for $(\mathbf{P}_{\text{RX-TX}}^\mathsf{T} \mathbf{P}_{\text{RX-TX}})^{-1}$ to be solvable requires $M \geq N$. Eq. (18) can be compactly expressed as

$$\hat{\bar{\mathbf{p}}}_{\text{T-TX}} = \mathbf{a} + \mathbf{B} \mathbf{r}_{\text{TX-T}} \qquad (19)$$

where $\mathbf{a} \triangleq \mathbf{P}^\dagger \mathbf{z}$ and $\mathbf{B} \triangleq \mathbf{P}^\dagger \mathbf{R}$.

Considering the block-diagonal structure of $\mathbf{P}_{\text{RX-TX}}$ in Eq. (6), we can write $\mathbf{P}^\dagger$ as

$$\mathbf{P}^\dagger = \begin{bmatrix} \mathbf{P}_1^\dagger & \ldots & \mathbf{0}_{N\times M} & \ldots & \mathbf{0}_{N\times M} \\ \vdots & \ddots & \vdots & \ddots & \vdots \\ \mathbf{0}_{N\times M} & \ldots & \mathbf{P}_l^\dagger & \ldots & \mathbf{0}_{N\times M} \\ \vdots & \ddots & \vdots & \ddots & \vdots \\ \mathbf{0}_{N\times M} & \ldots & \mathbf{0}_{N\times M} & \ldots & \mathbf{P}_L^\dagger \end{bmatrix}, \qquad (20)$$

thus allowing us to rewrite the $LN \times 1$ vector $\mathbf{a}$ in Eq. (19) as

$$\mathbf{a} = \begin{bmatrix} \mathbf{a}_1 \\ \vdots \\ \mathbf{a}_L \end{bmatrix} = \begin{bmatrix} \mathbf{P}_1^\dagger \mathbf{z}_1 \\ \vdots \\ \mathbf{P}_L^\dagger \mathbf{z}_L \end{bmatrix}, \qquad (21)$$

and the $NL \times L$ matrix $\mathbf{B}$ as

$$\mathbf{B} = \begin{bmatrix} \mathbf{b}_1 & \ldots & \mathbf{0}_{N\times 1} & \ldots & \mathbf{0}_{N\times 1} \\ \vdots & \ddots & \vdots & \ddots & \vdots \\ \mathbf{0}_{N\times 1} & \ldots & \mathbf{b}_l & \ldots & \mathbf{0}_{N\times 1} \\ \vdots & \ddots & \vdots & \ddots & \vdots \\ \mathbf{0}_{N\times 1} & \ldots & \mathbf{0}_{N\times 1} & \ldots & \mathbf{b}_L \end{bmatrix}, \qquad (22)$$

where $\mathbf{b}_l = \mathbf{P}_l^\dagger \mathbf{r}_l$ (an $N \times 1$ vector) is positioned between rows $N(l-1)+1$ and lN, and in column l. Expanding Eq. (19), the following equality is obtained:

$$\begin{bmatrix} \hat{\bar{\mathbf{p}}}_{\text{T-TX1}} \\ \vdots \\ \boxed{\hat{\bar{\mathbf{p}}}_{\text{T-TX}l}} \\ \vdots \\ \hat{\bar{\mathbf{p}}}_{\text{T-TX}L} \end{bmatrix} = \begin{bmatrix} \mathbf{a}_1 + \mathbf{b}_1 r_{\text{TX1-T}} \\ \vdots \\ \boxed{\mathbf{a}_l + \mathbf{b}_l r_{\text{TX}l\text{-T}}} \\ \vdots \\ \mathbf{a}_L + \mathbf{b}_L r_{\text{TX}L\text{-T}} \end{bmatrix}. \quad (23)$$

We expect to have $r_{\text{TX}l\text{-T}}^2 \approx ||\hat{\bar{\mathbf{p}}}_{\text{T-TX}l}||^2$, so that

$$r_{\text{TX}l\text{-T}}^2 \approx (\mathbf{a}_l + \mathbf{b}_l r_{\text{TX}l\text{-T}})^\mathsf{T} (\mathbf{a}_l + \mathbf{b}_l r_{\text{TX}l\text{-T}}). \quad (24)$$

Therefore, the estimate of $r_{\text{TX}l\text{-T}}$ can be seen as the solution of a simple second–degree equation:

$$\hat{r}_{\text{TX}l-\text{T}} = \frac{-2\mathbf{a}_l^\mathsf{T}\mathbf{b}_l \pm \sqrt{4(\mathbf{a}_l^\mathsf{T}\mathbf{b}_l)^2 - 4(\mathbf{b}_l^\mathsf{T}\mathbf{b}_l - 1)\mathbf{a}_l^\mathsf{T}\mathbf{a}_l}}{2(\mathbf{b}_l^\mathsf{T}\mathbf{b}_l - 1)}. \quad (25)$$

As shown in Eq. (25), there are two options for each $\hat{r}_{\text{TX}l-\text{T}}$, $l \in \mathcal{L}$. Therefore, we have, in total, 2^L possible estimates of vector $\mathbf{r}_{\text{TX-T}}$. All those estimates are evaluated in Eq. (18) to obtain the possible vectors of $\hat{\bar{\mathbf{p}}}_{\text{T-TX}}$. Those vectors are used to compute the cost function $\xi(\mathbf{x})$. The vector $\hat{\bar{\mathbf{p}}}_{\text{T-TX}}$ that obtains the lowest value of $\xi(\mathbf{x})$ is used to compute the final target estimate using Eq. (16).

C. Nonlinearly Constrained Least Square

The SI algorithm in Section II-A and the SX algorithm in Section II-B approximate the solution of Eq. (12) without considering the complete problem. The SI algorithm approaches Eq. (12) disregarding the nonlinear relationship of the entries of $\mathbf{x}$ ($||\hat{\bar{\mathbf{p}}}_{\text{T-TX}l}||$ should correspond exactly to $\hat{r}_{\text{TX}l-\text{T}}$). On the other hand, although the SX algorithm guarantees that $||\hat{\bar{\mathbf{p}}}_{\text{T-TX}l}|| = \hat{r}_{\text{TX}l\text{-T}}$, it does not necessarily satisfy the identity in Eq. (12).

In [8], a nonlinearly constrained least square (NLCLS) solution, defined for a scenario with M RXs and 1 TX, was proposed considering the complete mathematical problem in Eq. (12). By considering all the constraints of the original nonlinear problem in Eq. (12), the resulting method enjoys some regularization effects that implicitly compensate TDOA estimation errors, as corroborated by simulation results [8]. This section extends the NLCLS mathematical formulations to the generic case of M RXs and L TXs.

1) The NLCLS Method: We have L nonlinear constrained functions to satisfy the interdependence of the entries of $\mathbf{x}$ defined as

$$f_l(\mathbf{x}) = \mathbf{x}^\mathsf{T} \bar{\mathbf{I}}_l \mathbf{x} = 0, \quad l \in \mathcal{L}, \quad (26)$$

where the $L(N+1) \times L(N+1)$ matrix $\bar{\mathbf{I}}_l$ is given as

$$\bar{\mathbf{I}}_l = \begin{bmatrix} \bar{\mathbf{I}}_l^{\text{top}} & \mathbf{0}_{LN \times L} \\ \mathbf{0}_{L \times LN} & \bar{\mathbf{I}}_l^{\text{bottom}} \end{bmatrix}. \quad (27)$$

$$\bar{\mathbf{I}}_l^{\text{top}} = \begin{bmatrix} \mathbf{0}_{(l-1)N \times (l-1)N} & \mathbf{0}_{(l-1)N \times N} & \mathbf{0}_{(l-1)N \times (L-l)N} \\ \mathbf{0}_{N \times (l-1)N} & \mathbf{I}_{N \times N} & \mathbf{0}_{N \times (L-l)N} \\ \mathbf{0}_{(L-l)N \times (l-1)N} & \mathbf{0}_{(L-l)N \times N} & \mathbf{0}_{(L-l)N \times (L-l)N} \end{bmatrix}, \text{ and}$$

the $L \times L$ matrix $\bar{\mathbf{I}}_l^{\text{bottom}}$ has all its entries equal to zero, but the entry in row l and column l, which is equal to -1.

With the L constraints in Eq. (26), we can use Lagrange multipliers and write the following relation:

$$\nabla_{\mathbf{x}}\xi(\mathbf{x}) = \sum_{l=1}^{L} \lambda_l \nabla_{\mathbf{x}} f_l(\mathbf{x}), \quad (28)$$

where λ_l is the Lagrange multiplier for each constraint (L in total). Eq. (28) can be simplified to:

$$2(\mathbf{A}^\mathsf{T}\mathbf{A}\mathbf{x} - \mathbf{A}^\mathsf{T}\mathbf{z}) = 2\left(\sum_{l=1}^{L} \lambda_l \bar{\mathbf{I}}_l\right) \mathbf{x}. \quad (29)$$

An iterative numerical method can be used to solve Eq. (29). As in [8] and [27], the Newton–Raphson method is used here. We define vector $\mathbf{v}$, with unknown variables, as

$$\mathbf{v} = \begin{bmatrix} \hat{\mathbf{x}}^\mathsf{T} & \hat{\boldsymbol{\lambda}}^\mathsf{T} \end{bmatrix}^\mathsf{T}, \text{ where } \hat{\boldsymbol{\lambda}} = \begin{bmatrix} \hat{\lambda}_1 \dots \hat{\lambda}_L \end{bmatrix}^\mathsf{T} \quad (30)$$

and the vector $\mathbf{f}$, whose Euclidean norm must be minimized, is defined as

$$\mathbf{f} = \begin{bmatrix} \nabla_{\mathbf{x}}\xi(\hat{\mathbf{x}}) - \sum_{l=1}^{L} \hat{\lambda}_l \nabla_{\mathbf{x}} f_l(\hat{\mathbf{x}}) \\ f_1(\hat{\mathbf{x}}) - K_1 \\ \vdots \\ f_L(\hat{\mathbf{x}}) - K_L \end{bmatrix} = \begin{bmatrix} 2(\mathbf{A}^\mathsf{T}\mathbf{A}\hat{\mathbf{x}} - \mathbf{A}^\mathsf{T}\mathbf{z}) - 2\sum_{l=1}^{L} \hat{\lambda}_l \bar{\mathbf{I}}_l \hat{\mathbf{x}} \\ \hat{\mathbf{x}}^\mathsf{T} \bar{\mathbf{I}}_1 \hat{\mathbf{x}} \\ \vdots \\ \hat{\mathbf{x}}^\mathsf{T} \bar{\mathbf{I}}_L \hat{\mathbf{x}} \end{bmatrix}.$$
$$(31)$$

The iterative process minimizes $||\mathbf{f}_k||$ updating $\mathbf{v}_k$ at each iteration k:

$$\mathbf{v}_{k+1} = \mathbf{v}_k - \mathbf{J}^{-1}(\mathbf{v}_k)\mathbf{f}(\mathbf{v}_k), \quad (32)$$

where $\mathbf{J}(\mathbf{v}_k)$ is the Jacobian of $\mathbf{f}$ evaluated at $\mathbf{v}_k$:

$$\mathbf{J}(\mathbf{v}_k) = \begin{bmatrix} 2(\mathbf{A}^\mathsf{T}\mathbf{A} - \sum_{l=1}^{L} \hat{\lambda}_l \bar{\mathbf{I}}_l) & -2\bar{\mathbf{I}}_1\hat{\mathbf{x}} & \dots & -2\bar{\mathbf{I}}_L\hat{\mathbf{x}} \\ 2\hat{\mathbf{x}}^\mathsf{T}\bar{\mathbf{I}}_1 & 0 & \dots & 0 \\ \vdots & \vdots & \vdots & \vdots \\ 2\hat{\mathbf{x}}^\mathsf{T}\bar{\mathbf{I}}_L & 0 & \dots & 0 \end{bmatrix}. \quad (33)$$

The initial value $\mathbf{v}_0$ can be set with vector $\hat{\mathbf{x}}$ of the unconstrained LS solution as $\hat{\mathbf{x}}_0$, as defined in Eq. (14), and $[\hat{\boldsymbol{\lambda}}]_0 = \mathbf{0}_{L \times 1}$: $\mathbf{v}_0 = \left[\left((\mathbf{A}^\mathsf{T}\mathbf{A})^{-1}\mathbf{A}^\mathsf{T}\mathbf{z}\right)^\mathsf{T} \quad \mathbf{0}_{L \times 1}^\mathsf{T} \right]^\mathsf{T}$.[1] The iterative procedure stops when $||\mathbf{f}_k|| < \epsilon$, where ϵ represents the algorithm's tolerance.

2) Simplified Method: If Eq. (26) holds for all $l \in \mathcal{L}$ (i.e. $||\bar{\mathbf{p}}_{\text{T-TX}l}||$ corresponds exactly to $r_{\text{TX}l\text{-T}}$ for all $l \in \mathcal{L}$), then it follows that

$$\sum_{l=1}^{L} ||\bar{\mathbf{p}}_{\text{T-TX}l}||^2 - \sum_{l=1}^{L} r_{\text{TX}l\text{-T}}^2 = 0. \quad (34)$$

We propose a simplified version of the NLCLS (S-NLCLS)) scheme by replacing the L constraints in Eq. (26) with the following single nonlinear constraint function that guarantees that $f(\mathbf{x})$ corresponds to Eq. (34)

$$f(\mathbf{x}) = \mathbf{x}^\mathsf{T} \bar{\mathbf{I}}_{\text{c}} \mathbf{x} = 0, \quad (35)$$

---

[1] We use $[\hat{\boldsymbol{\lambda}}]_k$ to denote the estimated $\hat{\boldsymbol{\lambda}}$, Lagrange multiplier vector of the NLCLS algorithm, at iteration k; and we use $[\hat{\lambda}_l]_k$ to represent the estimated $\hat{\lambda}_l$, the element of $\hat{\boldsymbol{\lambda}}$ in row l, at iteration k.

where

$$\bar{\mathbf{I}}_c = \begin{bmatrix} \mathbf{I}_{NL \times NL} & \mathbf{0}_{NL \times L} \\ \mathbf{0}_{L \times NL} & -\mathbf{I}_{L \times L} \end{bmatrix}. \tag{36}$$

In order to use this simplified scheme to estimate the solution of Eq. (12), we have

$$\nabla_{\mathbf{x}} \xi(\mathbf{x}) = \lambda \nabla_{\mathbf{x}} f(\mathbf{x}), \tag{37}$$

where λ is the Lagrange multiplier. Eq. (37), after some algebraic manipulation, leads to

$$2(\mathbf{A}^\mathsf{T}\mathbf{A}\mathbf{x} - \mathbf{A}^\mathsf{T}\mathbf{z}) = 2\lambda\bar{\mathbf{I}}_c\mathbf{x}. \tag{38}$$

We also solve Eq. (38), as in Section II-C1, iteratively using Newton–Raphson method. Similarly, we define the corresponding vectors $\mathbf{v}$ and $\mathbf{f}$, and the matrix $\mathbf{J}(\mathbf{v}_k)$ as:

$$\mathbf{v} = \begin{bmatrix} \hat{\mathbf{x}}^\mathsf{T} & \hat{\lambda} \end{bmatrix}^\mathsf{T}, \tag{39}$$

$$\mathbf{f} = \begin{bmatrix} \nabla_{\mathbf{x}} \xi(\hat{\mathbf{x}}) - \lambda \nabla_{\mathbf{x}} f(\hat{\mathbf{x}}) \\ f(\hat{\mathbf{x}}) - K \end{bmatrix} = \begin{bmatrix} 2(\mathbf{A}^\mathsf{T}\mathbf{A}\hat{\mathbf{x}} - \mathbf{A}^\mathsf{T}\mathbf{z}) - 2\lambda\bar{\mathbf{I}}_c\hat{\mathbf{x}} \\ \hat{\mathbf{x}}^\mathsf{T}\bar{\mathbf{I}}_c\hat{\mathbf{x}} \end{bmatrix}, \tag{40}$$

and

$$\mathbf{J}(\mathbf{v}_k) = \begin{bmatrix} 2(\mathbf{A}^\mathsf{T}\mathbf{A} - \lambda\bar{\mathbf{I}}_c) & -2\bar{\mathbf{I}}_c\hat{\mathbf{x}} \\ 2\hat{\mathbf{x}}^\mathsf{T}\bar{\mathbf{I}}_c & 0 \end{bmatrix}. \tag{41}$$

The initial value $\mathbf{v}_0$ can be set with $\hat{\mathbf{x}}_0$ as defined in Eq. (14), and $[\lambda]_0 = 0$: $\mathbf{v}_0 = \left[\left((\mathbf{A}^\mathsf{T}\mathbf{A})^{-1} \mathbf{A}^\mathsf{T}\mathbf{z} \right)^\mathsf{T} \quad 0 \right]^\mathsf{T}.$[2]

The NLCLS and S-NLCLS methods are summarized in Algorithm 1.

The S-NLCLS method has a reduced computational complexity when compared to the NLCLS method. We can see it when obtaining the matrix $\mathbf{J}_k$ (for it has less $(L-1)$ rows and $(L-1)$ columns for the S-NLCLS) and vector $\mathbf{f}_k$ (it has less $(L-1)$ rows). As a result, $\mathbf{J}_k$ and $\mathbf{f}_k$ require less matrix sums and multiplications, and $\mathbf{v}_{k+1}$ has significantly less complexity since it involves the solution of a linear system of equations (or equivalently a matrix inversion, $\mathbf{J}_k^{-1}$). Such computations have a complexity in the order of n_M^3, with n_M representing the matrix size.

III. TDOA DATA SELECTION

The aforementioned location methods assume the knowledge of the bistatic range $r_{\mathrm{B}ml}$. In practice, this parameter is estimated, for instance, by using the TDOA measurement from the signals of each pair RXm–TXl, $\hat{\tau}_{ml}$, to get the bistatic range estimate $\hat{r}_{\mathrm{B}ml} \triangleq \hat{\tau}_{ml}c$, where c represents the speed of light. In some specific cases, due to effects like multipath propagation or line-of-sight (TX–RX) blocking, TDOA estimations present much higher errors. Those abnormal values are considered outliers. These outliers may yield inaccurate target estimations (even for the NLCLS methods); therefore, they must be detected and removed.

---

[2]We use $[\hat{\lambda}]_k$ to represent the estimated $\hat{\lambda}$, Lagrange multiplier of the S-NLCLS algorithm, at iteration k.

Algorithm 1: Nonlinearly constrained least square methods: NLCLS and S-NLCLS

Result: Estimated target position: $\hat{\mathbf{p}}_\mathrm{T}$

1 $k \leftarrow 0$;

2 $\underbrace{[\hat{\boldsymbol{\lambda}}]_0 \leftarrow \mathbf{0}_{L \times 1}}_{\text{NLCLS}}$ or $\underbrace{[\hat{\lambda}]_0 \leftarrow 0}_{\text{S-NLCLS}}$;

3 $\hat{\mathbf{x}}_0 \leftarrow (\mathbf{A}^\mathsf{T}\mathbf{A})^{-1} \mathbf{A}^\mathsf{T}\mathbf{z}$;

4 $\underbrace{\mathbf{v}_0 \leftarrow \begin{bmatrix} \hat{\mathbf{x}}_0 \\ [\hat{\boldsymbol{\lambda}}]_0 \end{bmatrix}}_{\text{NLCLS}}$ or $\underbrace{\mathbf{v}_0 \leftarrow \begin{bmatrix} \hat{\mathbf{x}}_0 \\ [\hat{\lambda}]_0 \end{bmatrix}}_{\text{S-NLCLS}}$;

5 **do**

6 $\quad k = k + 1$;

7 $\quad \mathbf{J}_k = \underbrace{\begin{bmatrix} 2(\mathbf{A}^\mathsf{T}\mathbf{A} - \sum_{l=1}^{L}[\hat{\lambda}_l]_k\bar{\mathbf{I}}_l) & -2\bar{\mathbf{I}}_1\hat{\mathbf{x}}_k & \dots & -2\bar{\mathbf{I}}_L\hat{\mathbf{x}}_k \\ 2\hat{\mathbf{x}}_k^\mathsf{T}\bar{\mathbf{I}}_1 & 0 & \dots & 0 \\ \vdots & \vdots & \vdots & \vdots \\ 2\hat{\mathbf{x}}_k^\mathsf{T}\bar{\mathbf{I}}_L & 0 & \dots & 0 \end{bmatrix}}_{\text{NLCLS}}$

$\quad$ or $\underbrace{\mathbf{J}_k = \begin{bmatrix} 2(\mathbf{A}^\mathsf{T}\mathbf{A} - [\hat{\lambda}]_k\bar{\mathbf{I}}_c) & -2\bar{\mathbf{I}}_c\hat{\mathbf{x}}_k \\ 2\hat{\mathbf{x}}_k^\mathsf{T}\bar{\mathbf{I}}_c & 0 \end{bmatrix}}_{\text{S-NLCLS}}$;

8 $\quad \mathbf{f}_k = \underbrace{\begin{bmatrix} 2(\mathbf{A}^\mathsf{T}\mathbf{A}\hat{\mathbf{x}}_k - \mathbf{A}^\mathsf{T}\mathbf{z}) - 2\sum_{l=1}^{L}[\hat{\lambda}_l]_k\bar{\mathbf{I}}_l\hat{\mathbf{x}}_k \\ \hat{\mathbf{x}}_k^\mathsf{T}\bar{\mathbf{I}}_1\hat{\mathbf{x}}_k \\ \vdots \\ \hat{\mathbf{x}}_k^\mathsf{T}\bar{\mathbf{I}}_L\hat{\mathbf{x}}_k \end{bmatrix}}_{\text{NLCLS}}$ or

$\quad \mathbf{f}_k = \underbrace{\begin{bmatrix} 2(\mathbf{A}^\mathsf{T}\mathbf{A}\hat{\mathbf{x}}_k - \mathbf{A}^\mathsf{T}\mathbf{z}) - 2[\hat{\lambda}]_k\mathbf{I}_c\hat{\mathbf{x}}_k \\ \hat{\mathbf{x}}_k^\mathsf{T}\mathbf{I}_c\hat{\mathbf{x}}_k \end{bmatrix}}_{\text{S-NLCLS}}$;

9 $\quad \mathbf{v}_{k+1} = \mathbf{v}_k - \mathbf{J}_k^{-1}\mathbf{f}_k$;

10 $\quad \hat{\mathbf{x}}_{k+1} \leftarrow$ first $(N+1)L$ entries of $\mathbf{v}_{k+1}$;

11 $\quad \underbrace{[\hat{\boldsymbol{\lambda}}]_{k+1} \leftarrow \text{last } L \text{ entries of } \mathbf{v}_{k+1}}_{\text{NLCLS}}$ or

$\quad \underbrace{[\hat{\lambda}]_{k+1} \leftarrow \text{last entry of } \mathbf{v}_{k+1}}_{\text{S-NLCLS}}$;

12 **while** $\|\mathbf{f}_k\| > \epsilon$;

13 $\hat{\bar{\mathbf{p}}}_{\text{T-TX}} \leftarrow$ first NL entries of $\mathbf{v}_{k+1}$;

14 $\hat{\mathbf{p}}_\mathrm{T} = (\mathbf{I}_a^\mathsf{T}\mathbf{I}_a)^{-1} \mathbf{I}_a^\mathsf{T} \left(\hat{\bar{\mathbf{p}}}_{\text{T-TX}} + \bar{\mathbf{p}}_{\text{TX}} \right)$;

A. Proposed Method: A Cuboid-based Search

Inspired by the works in [20] and [21], we propose the cuboid-based search (CS) method, which starts by dividing the location region, $\mathcal{V} \subset \mathbb{R}^N$,[3] into C_1 cuboids with dimensions $d_x^{(1)}$, $d_y^{(1)}$, and $d_z^{(1)}$.[4] Each individual cuboid, $\mathfrak{c}_i^{(1)}$, $i \in \mathfrak{C} \triangleq \{1, \dots, C_1\}$, is disjoint and connected with its neighbor cuboids. Fig. 2 shows an example of a PCL system, whose TXs and RXs have their positions given in Table I.

---

[3]For the forthcoming explanations, we shall consider here the more general case where $N = 3$.

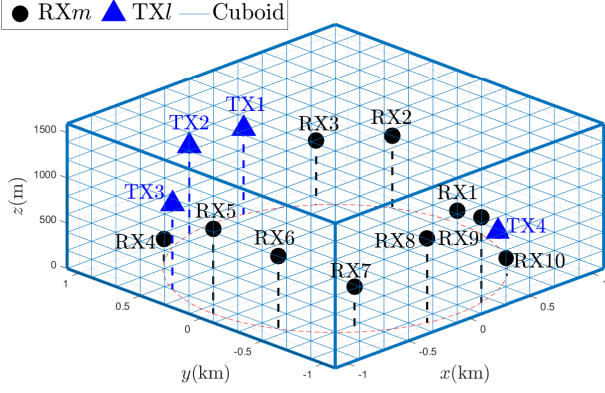[4]In this method, we use a superscript in parenthesis (s) to denote the first or second search, $s \in \{1, 2\}$

Fig. 2. PCL system with $M = 10$ RXs and $L = 4$ TXs. Positions of TXs and RXs are given in Table I. The location volume $\mathcal{V}$ has dimensions $(2.2 \times 2.2 \times 1.6)$ km^3 and is divided into $C_1 = 11 \times 11 \times 8 = 968$ cuboids with $d_x^{(1)} = d_y^{(1)} = d_z^{(1)} = 200$ m.
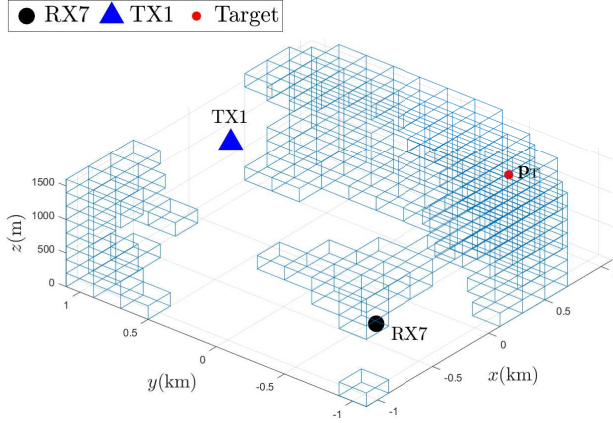

Fig. 3. Cuboids associated with a target location and a single TX-RX pair of the PCL system of Fig. 2 in the location volume $\mathcal{V}$ with dimensions $(2.2 \times 2.2 \times 1.6)$ km^3: RX7, TX1 and $\mathbf{p}_T = \begin{bmatrix} 840 & -559 & 1088 \end{bmatrix}^\mathsf{T}$.

Algorithm 2: Cuboid-based search

Result: outliers $o \in \mathcal{O}$ and selected TDOAs $t \in \mathfrak{T}$

1   $\mathcal{Q} \leftarrow \mathcal{V}$ $\triangleright$ initialize the search volume;

2   **for** all $s \in \mathfrak{S} \triangleq \{1, 2\}$ **do**

3   Split $\mathcal{Q}$ into cuboids of sizes $\left(d_x^{(s)}, d_y^{(s)}, d_z^{(s)} \right)$;

4     $i \in \mathfrak{C}_s \triangleq \{1, \ldots, C_s\}$ $\triangleright$ indexes of new cuboids $\mathfrak{c}_i^{(s)}$;

5   **for** all $i \in \mathfrak{C}_s$ **do**

6       $P_i^{(s)} \leftarrow 0$ $\triangleright$ initialize the counter per $\mathfrak{c}_i^{(s)}$;

7   **end**

8   **for** all $m \in \mathcal{M}$ **do**

9   **for** all $l \in \mathcal{L}$ **do**

10   **for** all $i \in \mathfrak{C}_s$ **do**

11         $\mathcal{T}_{ml}^{i(s)} = \left[\min \tau_{ml} \left(\mathfrak{c}_i^{(s)} \right), \max \tau_{ml} \left(\mathfrak{c}_i^{(s)} \right) \right]$;

12   **if** $\hat{\tau}_{ml} \in \mathcal{T}_{ml}^{i(s)}$ **then**

13          $P_i^{(s)} \leftarrow P_i^{(s)} + 1$ $\triangleright$ add the counter;

14   **end**

15   **end**

16   **end**

17   **end**

18     $\mathcal{W}_s \leftarrow \left\{ \underset{i \in \mathfrak{C}_s}{\arg\max} P_i^{(s)} \right\}$ $\triangleright$ winner cuboid(s)' index;

19     $\mathcal{Q} \leftarrow \mathfrak{c}_w^{(s)}, w \in \mathcal{W}_s$ $\triangleright$ new search volume;

20   **end**

21   $p_w^{\mathrm{cc}} \leftarrow$ center of cuboid(s) of $\mathfrak{c}_w^{(2)}, w \in \mathcal{W}_2$;

22   $\xi^{(w)}(\mathbf{x}) \leftarrow$ cost(s) associated with $p_w^{\mathrm{cc}}, w \in \mathcal{W}_2$;

23   $\bar{w} \leftarrow \left\{ \underset{w \in \mathcal{W}_2}{\arg\min} \xi^{(w)}(\mathbf{x}) \right\}$

24   $\mathfrak{c}_{\bar{w}}^{(2)} \leftarrow$ final winner cuboid;

25   $p_{\bar{w}}^{\mathrm{cc}} \leftarrow$ centroid of $\mathfrak{c}_{\bar{w}}^{(2)}$ and location estimation based on CENTROID-CS method;

26   $o \in \mathcal{O} \triangleq \{ \hat{\tau}_{ml} \notin \mathcal{T}_{ml}^{\bar{w}(2)}, \forall m \in \mathcal{M}, l \in \mathcal{L} \}$ $\triangleright$ outliers;

27   $t \in \mathfrak{T} \triangleq \{ \hat{\tau}_{ml} \in \mathcal{T}_{ml}^{\bar{w}(2)}, \forall m \in \mathcal{M}, l \in \mathcal{L} \}$ $\triangleright$ selected TDOAs;

The search region (volume) $\mathcal{V}$, with dimensions $(2.2 \times 2.2 \times 1.6)$ km^3, is split into $C_1 = 11 \times 11 \times 8 = 968$ cuboids with dimensions $d_x^{(1)} = d_y^{(1)} = d_z^{(1)} = 200$ m.

Each individual cuboid $\mathfrak{c}_i^{(1)}$ in $\mathcal{V}$ has a specific TDOA interval associated with each RXm–TXl pair: $\mathcal{T}_{ml}^{i(1)} \triangleq \left[\min \tau_{ml} \left(\mathfrak{c}_i^{(1)} \right), \max \tau_{ml} \left(\mathfrak{c}_i^{(1)} \right) \right] \subset \mathbb{R}$, where $\tau_{ml} \left(\mathfrak{c}_i^{(1)} \right) \subset \mathbb{R}$ is the set of all RXm–TXl TDOA nominal values for target locations in the cuboid $\mathfrak{c}_i^{(1)} \subset \mathcal{V}$. Geometrically, $\min \tau_{ml} \left(\mathfrak{c}_i^{(1)} \right)$ is related to the minimum bistatic range of the cuboid vertexes $\min r_{\mathrm{B}ml} \left(\mathfrak{c}_i^{(1)} \right)$ and $\max \tau_{ml} \left(\mathfrak{c}_i^{(1)} \right)$ is related to the maximum value $\max r_{\mathrm{B}ml} \left(\mathfrak{c}_i^{(1)} \right)$. For each RX$m$–TX$l$ pair, $m \in \mathcal{M}$ and $l \in \mathcal{L}$, a TDOA τ_{ml}, associated with a specific target location, $\mathbf{p}_T$, belongs to a group of cuboids that intersect the surface of an ellipsoid with foci associated with RXm and TXl, and a constant bistatic range $r_{\mathrm{B}ml}$. Fig. 3 shows the cuboids associated with the pair RX7-TX1 ($\tau_{71} = 4.16 \times 10^{-6}$ s) corresponding to the target position $\mathbf{p}_T = \begin{bmatrix} 840 & -559 & 1088 \end{bmatrix}^\mathsf{T}$, in meters, and the PCL system in Fig. 2. The cuboids in Fig. 3 intersect the ellipsoid whose

surfaces crosses $\mathbf{p}_T = \begin{bmatrix} 840 & -559 & 1088 \end{bmatrix}^\mathsf{T}$ m and with foci in RX7 and TX1 (one single pair).[5] Note that the complete solution in our tested scenario has 40 ellipsoids (coming from ML pairs of TXs and RXs).

The main principle underlying the CS method is to select the cuboid(s) that are intersected more times by the ellipsoids corresponding to the TDOA measurements $\hat{\tau}_{ml}$, for all $m \in \mathcal{M}$ and $l \in \mathcal{L}$. The winner cuboid(s) represents the new search volume, which will be further split into smaller cuboids of dimensions $d_x^{(2)}$, $d_y^{(2)}$, and $d_z^{(2)}$, where the TDOA selection is again performed. This second search gets a fine adjustment in the final selection. Algorithm 2 summarizes the TDOA selection process based on the CS method.

In case we have more than one winner cuboid as a result of the second search, we propose taking each cuboid's centroid as possible target locations to compute the cost function $\xi(\mathbf{x})$. The cuboid associated with the least cost is the final cuboid

---

[5]We do not see all cuboids that intercept the complete ellipsoid because Fig. 2 shows the cuboids in our PCL volume $\mathcal{V}$ with dimensions $(2.2 \times 2.2 \times 1.6)$ km^3

that classifies consistent data and outliers. In any case, the centroid of the selected cuboid can also be considered the target location estimate. Therefore, we name this estimate as CENTROID-CS.

B. Simple Choice Method

The simple choice (SC) method quickly classifies consistent TDOAs and outliers based on a comparison rule. Initially, we compute the target location (SI, SX, NLCLS or S-NLCLS method) considering all TDOAs. Then, this target location is used to obtain the bistatic range of each RXm–TXl pair, $r_{\mathrm{B}_{ml}}$, using Eq. (1). An estimate of $r_{\mathrm{B}_{ml}}$ can also be obtained employing the corresponding TDOA measurements: $\hat{r}_{\mathrm{B}_{ml}} = c\hat{\tau}_{ml}$.

The normalized error of bistatic range for each RXm–TXl pair is defined as

$$\eta_{ml} \triangleq \frac{\hat{r}_{\mathrm{B}_{ml}} - r_{\mathrm{B}_{ml}}}{r_{\mathrm{B}_{ml}}}. \tag{42}$$

In case we have an outlier, $\hat{r}_{\mathrm{B}_{ml}}$ will likely be much greater than $r_{\mathrm{B}_{ml}}$. However, it is only possible when we have a reasonable initial target estimation with outliers. As we will see in Section V, it only works properly with few outliers.

In order to determine if $\hat{\tau}_{ml}$ is an outlier, a decision rule is stated as

$$\eta_{ml} \underset{\hat{\tau}_{ml} \in \mathfrak{T}}{\overset{\hat{\tau}_{ml} \in \mathcal{O}}{\gtrless}} \alpha_{\mathrm{SC}}, \tag{43}$$

where α_{SC} is the threshold of the SC method. If η_{ml} is greater than α_{SC}, $\hat{\tau}_{ml}$ belongs to the outlier set $\mathcal{O}$. Otherwise, $\hat{\tau}_{ml}$ belongs to the selected set $\mathfrak{T}$.

C. Closest Neighbor Method

A closest neighbor (CN) method, as the one proposed in [25] and [26], discards outliers in an iterative process where one outlier is detected in each iteration. Initially, the outlier set $\mathcal{O}$ is empty and the selected set $\mathfrak{T}$ contains all TDOA measurements.

Subsequently, in each iteration, this method establishes a list of candidates for most likely outliers. The candidates are selected from set $\mathfrak{T}$, when the normalized error η_{ml} associated with the RXm–TXl pair follows the rule $\eta_{ml} > \mathrm{mean}(\eta_{ml})$ (this mean value is computed across the elements in the set $\mathfrak{T}$). For each candidate TDOA measurement, we estimate the target position discarding all TDOAs in $\mathcal{O}$ and the candidate itself. This target position serves to compute the cost function $\xi(\mathbf{x})$. The candidate associated with the maximum cost is classified as an outlier; consequently, included in the set $\mathcal{O}$ and removed from the set $\mathfrak{T}$.

The iterative process automatically stops, when the normalized errors η_{ml} of all TDOA measurements in the set $\mathfrak{T}$ follow the rule $\|\eta_{ml}\| < \alpha_{\mathrm{CN}}$, α_{CN} being the threshold of the CN method that ensures that there is not a considerable difference between the bistatic ranges $r_{\mathrm{B}_{ml}}$, computed employing the estimated target position, and its estimated versions $\hat{r}_{\mathrm{B}_{ml}}$, from the TDOA measurements. Algorithm 3 summarizes the TDOA selection process based on the CN method.

Algorithm 3: Closest Neighbor

Result: outliers $o \in \mathcal{O}$, selected TDOAs $t \in \mathfrak{T}$, and target location $\hat{\mathbf{p}}_{\mathrm{T}}$

1   $\mathcal{O} \leftarrow \emptyset$ and $\mathfrak{T} \leftarrow \{\hat{\tau}_{ml}, \forall m \in \mathcal{M}, l \in \mathcal{L}\}$;
2   Estimate $\hat{\mathbf{p}}_{\mathrm{T}}$;
3   Compute η_{ml} as in Eq. (42) for all $\tau_{ml} \in \mathfrak{T}$;
4   **while** any $\|\eta_{ml}\| > \alpha_{\mathrm{CN}}$ **do**
5     $g \in \mathcal{G} \triangleq \{\hat{\tau}_{ml} \in \mathfrak{T}|\eta_{ml} > \mathrm{mean}(\eta_{ml})\}$ $\triangleright$ candidate outliers;
6   **for** all $\hat{\tau}_{ml} \in \mathcal{G}$ **do**
7       $\hat{\mathbf{p}}_{\mathrm{T}}^{(ml)} \leftarrow$ estimated $\hat{\mathbf{p}}_{\mathrm{T}}$ discarding $\mathcal{O}$ and $\hat{\tau}_{ml}$;
8       $\xi^{(ml)}(\mathbf{x}) \leftarrow$ cost associated with $\hat{\mathbf{p}}_{\mathrm{T}}^{(ml)}$;
9   **end**
10   Add $\hat{\tau}_{ml}$ associated with $\max\left[\xi^{(ml)}(\mathbf{x})\right]$ to $\mathcal{O}$;
11   Exclude $\hat{\tau}_{ml}$ associated with $\max\left[\xi^{(ml)}(\mathbf{x})\right]$ from $\mathfrak{T}$;
12   Compute η_{ml} as in Eq. (42) for all $\hat{\tau}_{ml} \in \mathfrak{T}$;
13   Estimate $\hat{\mathbf{p}}_{\mathrm{T}}$ discarding $\hat{\tau}_{ml} \in \mathcal{O}$;
14 **end**

IV. TARGET LOCATION DISCARDING OUTLIERS

PCL algorithms need a proper TDOA selection to attain good accuracy. Therefore, the target estimation algorithms do not use the data associated with TDOA measurements that belong to the outlier set $\mathcal{O}$. Consequently, we have the following modifications:

1) In each matrix $\bar{\mathbf{P}}_{\mathrm{RX\text{-}TX}l}$, $l \in \mathcal{L}$, which is part of matrix $\mathbf{P}_{\mathrm{RX\text{-}TX}}$, remove the rows $\bar{\mathbf{p}}_{\mathrm{RX}m\text{-}\mathrm{TX}l}^{\mathsf{T}}$ whose TX/RX pairs are associated with indexes in $\mathcal{O}$.
2) In each vector $\mathbf{r}_l$, which is part of matrix $\mathbf{R}$, remove the rows r_{ml} associated with $o \in \mathcal{O}$.
3) In each vector $\mathbf{z}_l$, $l \in \mathcal{L}$, which is part of vector $\mathbf{z}$, remove the rows associated with $o \in \mathcal{O}$.
4) For each TXl, $l \in \mathcal{L}$, verify the amount of selected $\hat{\tau}_{ml}$, $\hat{\tau}_{ml} \notin \mathcal{O}$: $M_l^{\bullet}$ (not considering the outliers).
5) In case $M_l^{\bullet} < N + 1$ for SI, NLCLS and S-NLCLS, or $M_l^{\bullet} < N$ for SX, $l \in \mathcal{L}$, remove the columns associated with matrix $\bar{\mathbf{P}}_{\mathrm{RX\text{-}TX}l}$ in $\mathbf{P}_{\mathrm{RX\text{-}TX}}$, remove the column l in matrix $\mathbf{R}$ and remove the rows associated with $\mathbf{z}_l$ in $\mathbf{z}$.

The PCL algorithms investigated herein (SX, SI, NLCLS and S-NLCLS) use the modified versions of vector $\mathbf{z}$ and matrices $\mathbf{P}_{\mathrm{RX\text{-}TX}}$ and $\mathbf{R}$ to compute the target location. This solution (that does not take into consideration the outliers in $\mathcal{O}$) can only be obtained when there exists at least one $l \in \mathcal{L}$ for which $M_l^{\bullet} \geq N + 1$ for SI, NLCLS and S-NLCLS, or $M_l^{\bullet} \geq N$ for SX. Otherwise, the solution is incomplete, and the estimation computation uses all TDOAs.

V. EXPERIMENTAL RESULTS

A. Simulation Scenario

We assessed the PCL algorithms and the TDOA selection techniques in the simulated 3D PCL scenario of Fig. 2, considering $N_{\mathrm{p}} = 75$ theoretical target locations. Vector $\mathbf{p}_{\mathrm{T}}(n_{\mathrm{p}}) = \begin{bmatrix} x_{\mathrm{T}}(n_{\mathrm{p}}) & y_{\mathrm{T}}(n_{\mathrm{p}}) & x_{\mathrm{T}}(n_{\mathrm{p}}) \end{bmatrix}^{\mathsf{T}}$, $n_{\mathrm{p}} \in \mathcal{P} \triangleq \{1, 2, \ldots, N_{\mathrm{p}}\}$,
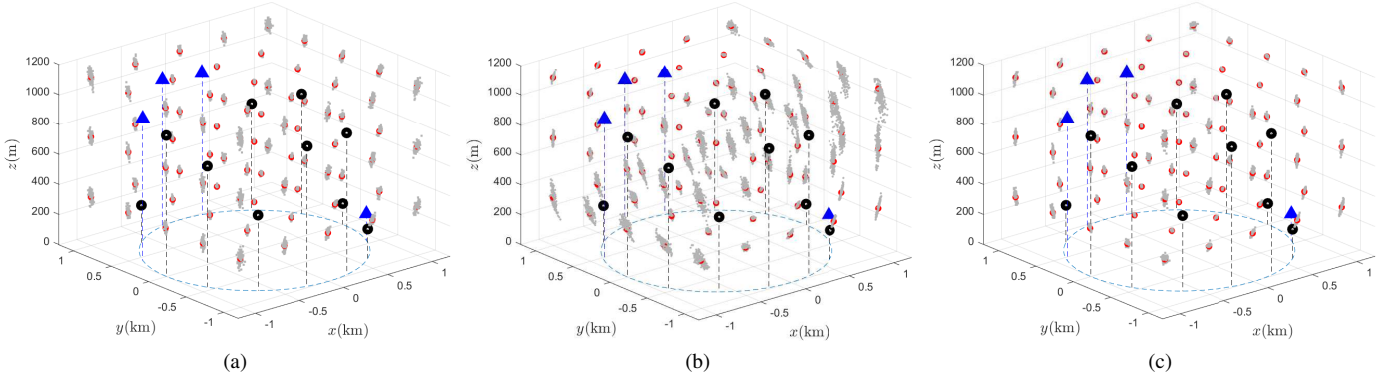
Fig. 4. Target location estimations in the PCL system of Fig. 2 without outliers. Transmitters in blue, receivers in black, theoretical target positions in red, and estimated target positions in grey. (a) SI method, (b) SX method, and (c) NLCLS method.

TABLE I
POSITIONS OF TXs AND RXs OF THE PCL SYSTEM SHOWN IN FIGURE 2

	RX1	RX2	RX3	RX4	RX5	RX6	RX7	RX8	RX9	RX10	TX1	TX2	TX3	TX4
x(m)	1000	901	623	-623	-1000	-901	-623	-223	223	623	223	-223	-901	901
y(m)	0	434	782	782	0	-434	-782	-975	-975	-782	975	975	434	-434
z(m)	139	800	712	247	938	805	502	932	942	195	947	979	947	177

represents the n_{p}-th target location. The $N_{\mathrm{p}} = 75$ theoretical target locations corresponds to all combinations of $x_{\mathrm{T}}(n_{\mathrm{p}})$, $y_{\mathrm{T}}(n_{\mathrm{p}})$, and $z_{\mathrm{T}}(n_{\mathrm{p}})$ taken from:

- $x_{\mathrm{T}}(n_{\mathrm{p}}) \in \mathcal{X} \triangleq \{-1025, -525, -25, 475, 975\}$ m,
- $y_{\mathrm{T}}(n_{\mathrm{p}}) \in \mathcal{Y} \triangleq \{-1020, -520, -20, 480, 980\}$ m, and
- $z_{\mathrm{T}}(n_{\mathrm{p}}) \in \mathcal{Z} \triangleq \{330, 731.5, 1133\}$ m.

To evaluate the behavior of the proposed methods, we executed $N_{\mathrm{r}} = 100$ independent runs on each of the $N_{\mathrm{p}} = 75$ theoretical target positions. As a result, a numerical assessment was performed on each target position using the root mean square error (RMSE):

$$\mathrm{RMSE}(n_{\mathrm{p}}) = \sqrt{\frac{1}{N_{\mathrm{r}}} \sum_{k=1}^{N_{\mathrm{r}}} \left\| \mathbf{p}_{\mathrm{T}}(n_{\mathrm{p}}) - \hat{\mathbf{p}}_{\mathrm{T}}^{(k)}(n_{\mathrm{p}}) \right\|^2}, \quad (44)$$

where $\hat{\mathbf{p}}_{\mathrm{T}}^{(k)}(n_{\mathrm{p}})$ is the k-th estimate of $\mathbf{p}_{\mathrm{T}}(n_{\mathrm{p}})$. In the computation of $\mathrm{RMSE}(n_{\mathrm{p}})$, we considered 95% of the closest estimations of the theoretical target location $\mathbf{p}_{\mathrm{T}}(n_{\mathrm{p}})$. The global RMSE, which evaluates the location estimates in all theoretical target positions, is defined as

$$\mathrm{RMSE}_{\mathrm{G}} = \sqrt{\frac{1}{N_{\mathrm{p}}} \sum_{n_{\mathrm{p}}=1}^{N_{\mathrm{p}}} [\mathrm{RMSE}(n_{\mathrm{p}})]^2}. \quad (45)$$

These RMSE values represent accuracy indicators in the location estimation. Firstly, we tested the proposed location algorithms in simulated scenarios with TDOAs and considered no outliers. Subsequently, we included corrupted TDOAs in our PCL scenario to apply data selection for removing outliers before computing the target location.

B. Location Algorithm Evaluation

Each theoretical target position $\mathbf{p}_{\mathrm{T}}(n_{\mathrm{p}})$, $n_{\mathrm{p}} \in \mathcal{P}$, has ML associated theoretical TDOAs τ_{ml}, $m \in \mathcal{M}$ and $l \in \mathcal{L}$. We artificially disturbed each τ_{ml} by adding Gaussian noise with

zero mean and standard–deviation equivalent to $\sigma_\tau = 1\%$ of the same τ_{ml}. These artificial disturbances emulated the background noise present in TDOA measurements τ_{ml} due to sensor and signal impairments. The applied TDOA disturbances depend on bistatic range distances. The authors in [28] proved that the TDOA background noise varies according to source-to-sensor distances in a more realistic TDOA-based source location scenario.

We evaluated the location algorithms, described in Section II, using the TDOA measurements $\hat{\tau}_{ml}$ of all RX–TX pairs and considered no outliers. Fig. 4 shows the location estimates of the 75 theoretical target positions using methods SI, SX, and NLCLS. We omitted the S-NLCLS results, for they were virtually the same of the NLCLS algorithm. In all our experiments, the Newton method, in the same way as in [8], converged in a few iterations for both the S-NLCLS and NLCLS algorithms. The convergence was achieved in no more than ten iterations.

As seen in Fig. 4c, the NLCLS method presents smaller and less spread regions around the theoretical target positions, confirming that this method compensates SI estimations and reduces the impact of TDOA measurement errors. On the other hand, the SX method shows more prominent and elongated regions around the theoretical target positions, especially outside the convex hull associated with the locations of TXs and RXs. The global RMSE values of the SI, SX, S-NLCLS, and NLCLS methods were 17.65, 30.82, 14.31, and 14.14 m, respectively.

C. Location Algorithm Evaluation with Data Selection

In the following, we emulated outliers usually present in TDOA measurements due to effects such as lack of line-of-sigh (TX-RX) or multipath propagation. Then, based on a defined probability of occurrence P_{outlier}, a uniformly-distributed random variable (representing the outlier), distributed between 50% and 100% of τ_{ml}, was added to each nominal τ_{ml}, $m \in \mathcal{M}$ and $l \in \mathcal{L}$. In this case, the nominal τ_{ml} with the added uniform variable and the previously added Gaussian variable generated the measurement $\hat{\tau}_{ml}$. We also carried out $N_{\mathrm{r}} = 100$ independent runs for each of the 75 theoretical target positions, considering TDOA measurements with both background noise and outliers at different levels of probability

TABLE II

TOTAL RMSE$_G$ (IN BLUE) FOR TARGET LOCATION WITH TDOA SELECTION TECHNIQUE: CUBOID-BASED SEARCH (CS), WHERE d_1, d_2 AND RMSE$_G$ ARE GIVEN IN meters. OUTLIERS EVALUATED AT DIFFERENT PROBABILITIES OF OCCURRENCE, $P_{\text{outlier}} \in \mathcal{P}_O$.

|	d_1	366.7	275.0	275.0	220.0	220.0	200.0	200.0	200.0	200.0	200.0	100.0	100.0	50.0	50.0
	d_2	183.3	137.5	68.8	110.0	73.3	100.0	66.7	50.0	40.0	25.0	50.0	33.3	25.0	16.7
SI-CS	RMSE$_G$	138.4	98.3	108.4	77.4	92.6	72.3	80.4	97.3	122.8	173.4	42.9	44.7	34.5	38.8
S-NLCLS-CS	RMSE$_G$	106.3	72.3	74.1	56.1	59.3	52.9	52.1	59.1	69.7	91.8	27.5	27.6	21.1	20.8
NLCLS-CS	RMSE$_G$	101.6	69.5	72.7	54.1	56.9	51.4	50.6	57.8	68.6	91.3	25.7	25.4	19.0	19.0
CENTROID-CS	RMSE$_G$	206.8	148.2	123.3	117.1	101.9	105.3	89.8	78.1	79.8	77.7	29.9	31.0	21.7	14.6
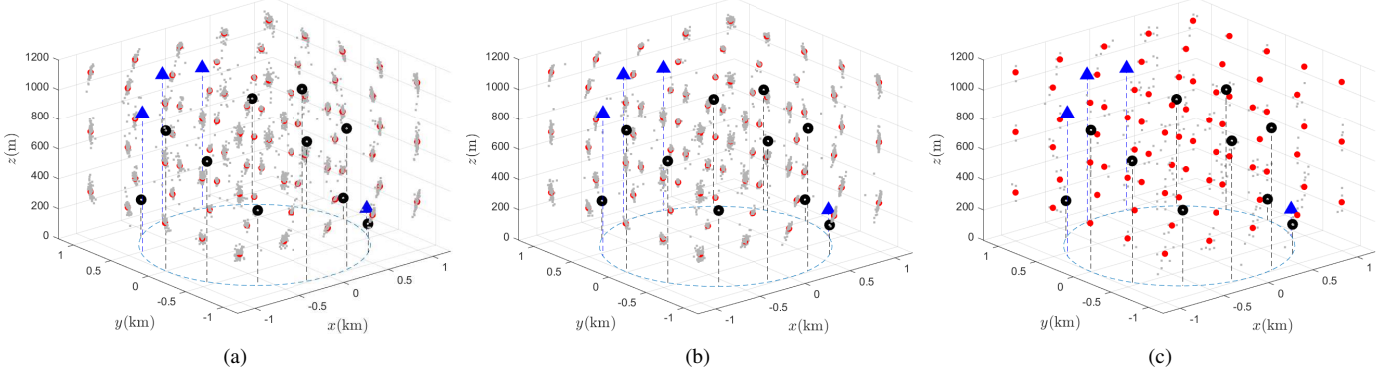
Fig. 5. Target location estimations with TDOA selection in the PCL system of Fig. 2 with outliers. Transmitters in blue, receivers in black, theoretical target positions in red, and estimated target positions in grey. P_{outlier}=0.3. (a) NLCLS-CN method: $\alpha_{\text{CN}} = 0.15$, (b) NLCLS-CS method: $d_1 = 100$ m and $d_2 = 50$ m, and (c) CENTROID-CS: $d_1 = 100$ m and $d_2 = 50$ m.

TABLE III

PCL LOCATION ALGORITHMS WHEN APPLYING TDOA DATA SELECTION

PCL location algorithms	TDOA selection technique	Location algorithms with data selection
Spherical Interpolation (SI)	Simple Comparison (SC)	SI-SC
	Closest Neighbor (CN)	SI-CN
	Cuboid-Search (CS)	SI-CS
Spherical Intersection (SX)	Simple Comparison (SC)	SX-SC
	Closest Neighbor (CN)	SX-CN
	Cuboid-Search (CS)	SX-CS
Nonlinearly Constrained Least Square (NLCLS)	Simple Comparison (SC)	NLCLS-SC
	Closest Neighbor (CN)	NLCLS-CN
	Cuboid-Search (CS)	NLCLS-CS
Simplified NLCLS (S-NLCLS)	Simple Comparison (SC)	S-NLCLS-SC
	Closest Neighbor (CN)	S-NLCLS-CN
	Cuboid-Search (CS)	S-NLCLS-CS

of occurrence, $P_{\text{outlier}} \in \mathcal{P}_O \triangleq \{0.0, 0.1, 0.2, 0.3, 0.4, 0.5\}$. In our experiments, we applied the TDOA selection techniques for the SI, S-NLCLS, and NLCLS algorithms, as seen in Table III. These methods showed better accuracy than the SX in the 3D PCL scenario depicted in Fig. 4.

To find the best threshold values for methods CN and SC, we carried out individual experiments, varying the thresholds between 0 and 0.7 and looking at the global RMSE. The designated thresholds are associated with the minimum RMSE$_G$ value. The selected thresholds using NLCLS were $\alpha_{\text{SC}} = 0.05$ and $\alpha_{\text{CN}} = 0.15$. The associated total RMSE$_G$ values were 173.56 m and 57.92 m, respectively, for NLCLS-SC and NLCLS-CN. On the other hand, using the SC and CN TDOA selection techniques with the S-NLCLS algorithm, the selected thresholds were $\alpha_{\text{SC}} = \alpha_{\text{CN}} = 0.1$. S-NLCLS-SC obtained RMSE$_G = 193.22$ m. SI-CN obtained RMSE$_G = 89.98$ m. Finally, using the SC and the CN techniques with the SI algorithm, the selected thresholds were $\alpha_{\text{SC}} = 0.05$ and $\alpha_{\text{CN}} = 0.35$. SI-SC obtained RMSE$_G = 515.10$ m. SI-CN

obtained RMSE$_G = 256.06$ m.

When applying the CS selection procedure, our simulations used cuboids with equal sizes: $d_1 = d_x^{(1)} = d_y^{(1)} = d_z^{(1)}$ for the bigger cuboids and $d_2 = d_x^{(2)} = d_y^{(2)} = d_z^{(2)}$ for the smaller cuboids. Table II shows the results of total RMSE$_G$ of different cuboid sizes for SI-CS, S-NLCLS-CS, NLCLS-CS, and CENTROID-CS. We also tested the mentioned CS procedures at different levels of probability of occurrence, $P_{\text{outlier}} \in \mathcal{P}_O$.

The cuboid sizes are of paramount importance in the final performance. The bigger cuboids select the region where the target is located, and the smaller cuboids perform the fine adjustment and the final TDOA selection. In Table II, we see that NLCLS-CS has better RMSE$_G$ results than all S-NLCLS-CS, SI-CS results, and most CENTROID-CS results. CENTROID-CS also gets good results, especially when reducing d_1 and d_2. One of the issues of reducing the cuboid sizes too much is that the processing load increases. Therefore, a good balance between RMSE$_G$ and processing load is necessary for practical implementations. For our PCL system, we consider suitable cuboid sizes $d_1 = 100$ m and $d_2 = 50$ m. Their associated RMSE$_G$ values were 42.9, 27.5, 25.7, and 29.9 m, respectively, for SI-CS, NLCLS-CS, NLCLS-CS, and CENTROID-CS.

Fig. 5 shows target estimates in the 75 theoretical target points of the PCL system of Fig. 2, considering $P_{\text{outlier}} = 0.3$. Fig. 5a, Fig. 5b, and Fig. 5c show, respectively, the target estimates for NLCLS-CN when $\alpha_{\text{CN}} = 0.15$, NLCLS-CS when $d_1 = 100$ and $d_2 = 50$ m, and CENTROID-CS when $d_1 = 100$ and $d_2 = 50$ m. The associated RMSE$_G$ values were 23.05, 20.07, and 26.19 m for NLCLS-CN, NLCLS-CS, and CENTROID-CS.

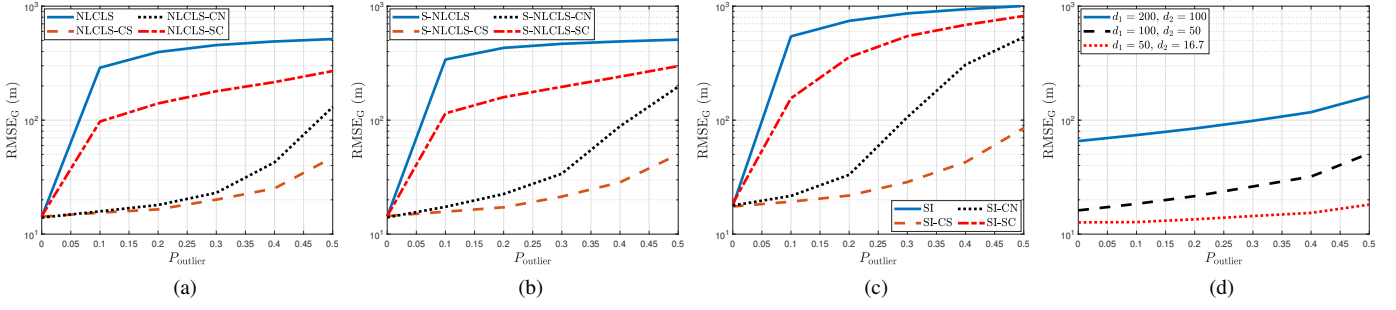Fig. 6 shows different RMSE$_G$ vs. P_{outlier} plots to analyze

Fig. 6. RMSE$_G$ vs. Probability of outlier (a) NLCLS, NLCLS-CS, NLCLS-CN and NLCLS-SC, (b) S-NLCLS, S-NLCLS-CS, S-NLCLS-CN and S-NLCLS-SC, (c) SI, SI-CS, SI-CN and SI-SC, and (d) CENTROID-CS.
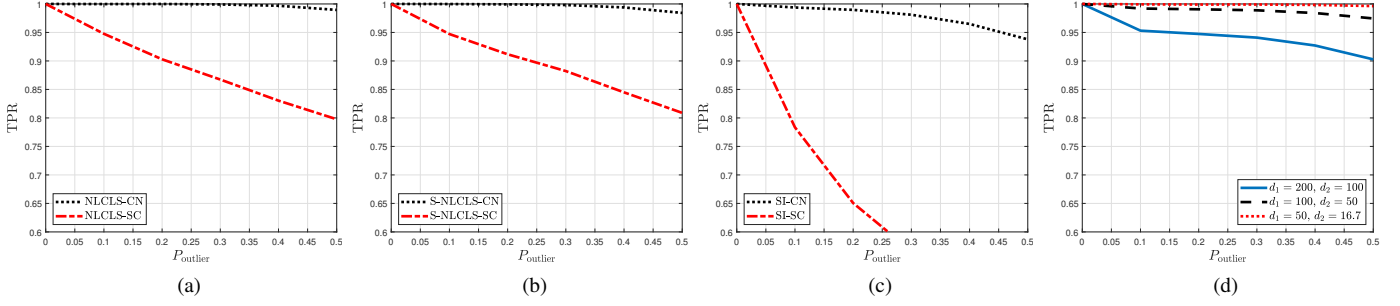

Fig. 7. TPR vs. $P_{outlier}$ (a) NLCLS-CN and NLCLS-SC, (b) S-NLCLS-CN and S-NLCLS-SC, (c) SI-CN and SI-SC, and (d) CS.
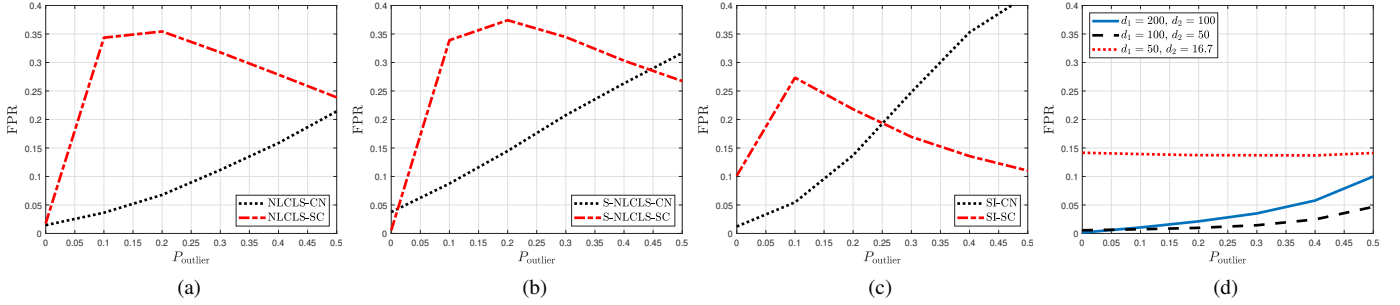

Fig. 8. FPR vs. $P_{outlier}$ (a) NLCLS-CN and NLCLS-SC, (b) S-NLCLS-CN and S-NLCLS-SC, (c) SI-CN and SI-SC, and (d) CS.

the techniques' accuracy in overcoming outliers at different probabilities of occurrence. Fig. 6a shows the plots for NL-CLS, NLCLS-SC ($\alpha_{SC} = 0.05$), NLCLS-CN ($\alpha_{CN} = 0.15$), and NLCLS-CS ($d_1 = 100$ and $d_2 = 50$ m). Fig. 6b shows the plots of RMSE$_G$ vs. $P_{outlier}$ for S-NLCLS, S-NLCLS-SC ($\alpha_{SC} = 0.1$), S-NLCLS-CN ($\alpha_{CN} = 0.1$), and SI-CS ($d_1 = 100$ and $d_2 = 50$ m). Fig. 6c shows the plots of RMSE$_G$ vs. $P_{outlier}$ for SI, SI-SC ($\alpha_{SC} = 0.05$), SI-CN ($\alpha_{CN} = 0.35$), and SI-CS ($d_1 = 100$ and $d_2 = 50$ m).

We see, in Fig. 6a, that NLCLS-CS best mitigated the effect of outliers and reduced RMSE$_G$. For example, in high $P_{outlier}$ values of 0.4 and 0.5, the associated RMSE$_G$ were, respectively, 25.17 and 47.15 m. On the other hand, NLCLS-CN effectively overcame (considering RMSE$_G \leq 50$ m as good accuracy) the outlier presence when $P_{outlier} \leq 0.41$. Considering the same accuracy level as NLCLS cases, we can see, in Fig. 6b , that S-NLCLS-CN and S-NLCLS-CS effectively mitigated the outlier presence, respectively, when $P_{outlier} \leq 0.34$ and $P_{outlier} \leq 0.50$. As seen in Fig. 6c, SI-CN and SI-CS overcame the outlier presence, respectively, when $P_{outlier} \leq 0.24$ and $P_{outlier} \leq 0.42$. NLCLS-SC, S-NLCLS-SC, and SI-SC only reduced the outlier effect compared,

respectively, to NLCLS, S-NLCLS, and SI. However, it was not possible to get good accuracy.

Fig. 6d shows the plots of RMSE$_G$ vs. $P_{outlier}$ for CENTROID-CS. We have 3 cases of (d_1, d_2): $(200, 100)$, $(100, 50)$, and $(50, 16.7)$ m. With cuboid sizes of $(50, 16.7)$ m, we obtained the best accuracy (RMSE$_G \leq 18.14$ m). However, because of its high number of comparisons (61952 per TX-RX pair in the first search and at least 8 per TX-RX pair in the second search) due to the small cuboid sizes (comparing with our tested location region $\mathcal{V}$ as seen in Fig. 2), it requires a high processing load. With cuboid sizes of $(100, 50)$ m, we also obtained good accuracy RMSE$_G \leq 50$ m using less comparisons (7744 per TX-RX pair in the first search and at least 8 per TX-RX pair in the second pair) and less processing.

We also corroborate RMSE$_G$ results with two crucial indicators:

- True positive rate (TPR) represents the probability that the TDOA is considered as an outlier when it indeed is an outlier.
- False positive rate (FPR) constitutes the probability that the TDOA is considered an outlier when it is not an outlier.

Fig. 7 shows TPR vs. P_{outlier} plots associated with RMSE_G results of Fig. 6. Fig. 8 shows FPR vs. P_{outlier} plots associated with RMSE_G results of Fig. 6. Generally, good RMSE_G results are associated with high TPR and low FPR rates. However, TPR rates have a higher incidence in the final location estimation accuracy. It means that the presence of an outlier in the target location estimation has a hig her interference than the absence of few consistent data. We can see it in the CENTROID-CS case with $d_1 = 50$ and $d_2 = 16.7$: $\text{RMSE}_G < 18.14$ m. It had an associated TPR> 0.996 and almost constant FPR≈ 0.14.

Based on our numerical results in the simulated PCL scenario, cuboid-based methods (NLCLS-CS, S-NLCLS-CS, SI-CS, and CENTROID-CS) overcame the outlier effects better than CN and SC. The effectiveness was demonstrated with lower RMSE_G values, higher TPR rates, and lower FPR rates. Outlier selection in these CS methods does not depend on the location algorithm. The applied location methods helped us obtain better accuracy in the final location estimation. Consequently, NLCLS-CS got better results than S-NLCLS-CS and SI-CS. On the other hand, CENTROID-CS directly obtained reasonable estimates representing the selected cuboid's centroid.

Conversely, CN methods depend on the applied location algorithms in the outlier selection procedure. Consequently, NLCLS-CN obtained better results. Generally, CN methods had good results; however, when increasing the P_{outlier} ($P_{\text{outlier}} > 0.24$ for SI-CN, $P_{\text{outlier}} > 0.34$ for S-NLCLS-CN, and $P_{\text{outlier}} > 0.41$ for NLCLS-CN), we can see a decrease of TPR, a rapid increase of FPR, and consequently a considerable decrease of RMSE_G. Finally, SC methods (NLCLS-SC, S-NLCLS-SC, and SI-SC) are simpler and have lower processing load (one simple comparison) than the other methods; however, they have lower accuracy. They could be useful only in case P_{outlier} was low ($P_{\text{outlier}} < 0.05$).

VI. CONCLUSION

Modern PCL environments using advanced radio networks, such as massive MIMO 5G NR with millimetric waves, require scenarios with multiple TXs/RXs. We started this work by formulating the SI, SX, and NLCLS algorithms that use TDOAs associated with multiple TXs/RXs systems. The authors in [7] and [8] introduced these algorithms for environments with multiple–TXs/one–RX and multiple–RXs/one–TX.

Location techniques based on electromagnetic radio waves can suffer effects like multipath propagation and shadow fading. Those effects corrupt TDOA measurements yielding considerable errors in the estimation of the target position. This paper showed that applying TDOA selection techniques improves the accuracy of the target location. Numerical experiments also corroborated that high TPR and low FPR rates in the outliers' detection task lead to good accuracy in the final estimation.

The best-performing proposed selection technique (CS) divides the location region into cuboids and discards the TDOAs measurements whose associated bistatic ranges are outside the cuboid that most likely contains consistent TDOAs. The center of the selected cuboid is considered another location estimation (CENTROID-CS). A significant contribution is that CENTROID-CS estimation does not add computational load considering that it is part of the original selection process. In the tested PCL scenario, NLCLS-CS, S-NLCLS-CS and CENTROID-CS showed to be effective in all cases ($P_{\text{outlier}} \leq 0.5$). SI-CS was effective when $P_{\text{outlier}} \leq 0.42$. The recommended cuboid sizes, considering the environment of interest and the processing load, were $d_1 = 100$ m and $d_2 = 50$ m.

On the other hand, CN excludes outliers using an iterative process that compares the cost functions of some candidates. This process resulted to be effective until a specific boundary: $P_{\text{outlier}} \leq 0.24$ for SI-CN, $P_{\text{outlier}} \leq 0.34$ for S-NLCLS-CN, and $P_{\text{outlier}} \leq 0.41$ for NLCLS-CN. Finally, the SC method quickly detects outliers based on a simple comparison rule. However, this method resulted to be effective only when a few outliers were present ($P_{\text{outlier}} \leq 0.05$).

REFERENCES

[1] M. Malanowski, *Signal Processing for Passive Bistatic Radar*, 1st ed. Artech House, 2019.

[2] H. Griffiths and C. Baker, *An Introduction to Passive Radar*. Artech House, 2017.

[3] H. Griffiths and C. Baker, "Passive coherent location radar systems. Part 1: Performance prediction," *IEE Proceedings - Radar, Sonar and Navigation*, vol. 152, no. 3, pp. 153–159, Jun. 2005.

[4] A. Aubry, A. D. V. Carotenuto, and L. Pallotta, "Joint exploitation of TDOA and PCL techniques for two-dimensional target localization," *IEEE Transactions on Aerospace and Electronic Systems*, vol. 56, no. 1, pp. 597–609, Feb. 2020.

[5] S. A. Kaiser, "Multistatic passive coherent location using the global position system," Ph.D. dissertation, The Pennsylvania State University - College of Engineering, 2017.

[6] L. Jinga, Z. Yongjuna, and L. Donghai, "Accurate single-observer passive coherent location estimation based on TDOA and DOA," *Chinese Journal of Aeronautics*, vol. 27, no. 4, pp. 913–923, Aug. 2014.

[7] M. Malanowski and K. Kulpa, "Two methods for target localization in multistatic passive radar," *IEEE Transactions on Aerospace and Electronic Systems*, vol. 48, no. 1, pp. 572–580, Jan. 2012.

[8] D. P. Nicolalde-Rodríguez, J. A. Apolinário Jr., and W. A. Martins, "Robust passive coherent location via nonlinearly constrained least squares," *Latin American Symposium on Circuits and Systems (LASCAS 2021)*, Feb. 2021.

[9] D. P. Nicolalde-Rodríguez, W. A. Martins, J. A. Apolinário Jr., and L. P. Caloba, "Localização coerente passiva de um alvo usando redes neurais feedforward - in Portuguese," *XXXIX Simpósio Brasileiro de Telecomunicações e Processamento de Sinais (SBrT 2021)*, Sep. 2021.

[10] S. Pak, B. Chalise, and B. Himed, "Target localization in multi-static passive radar systems with artificial neural networks," *International Radar Conference (RADAR)*, pp. 1–5, Sep. 2019.

[11] A. Dersan and Y. Tanik, "Passive radar localization by time difference of arrival," *IEEE Military Communications Conference (MILCOM) 2002*, Oct. 2002.

[12] W. Xiong, J. Bordoy, C. Schindelhauer, A. Gabbrielli, G. Fischer, D. Schott, F. Hoeflinger, S. Rupitsch, and H. So, "Data–Selective Least Squares Methods for Elliptic Localization with NLOS Mitigation," *IEEE Sensors Letters*, vol. 5, no. 7, pp. 1–4, Jul. 2021.

[13] C. Oestges and F. Quitin, *Inclusive Radio Communications for 5G and Beyond*, 1st ed. Elsevier, 2021.

[14] R. S. Thomä, C. Andrich, G. D. Galdo, M. Dobereiner, M. A. Hein, M. Kaske, G. Schafer, S. Schieler, C. Schneider, A. Schwind, and P. Wendland, "Cooperative passive coherent location: A promising 5G service to support road safety," *IEEE Communications Magazine*, vol. 57, no. 9, pp. 86–92, Sep. 2019.

[15] P. Samczyński, K. Abratkiewicz, M. Płotka, T. P. Zieliński, J. Wszołek, S. Hausman, P. Korbel, and A. Księżyk, "5G Network-Based Passive Radar," *IEEE Transactions on Geoscience and Remote Sensing*, vol. 60, pp. 1–9, 2022.

[16] M. Schwartz, *Characteristics of the mobile radio environment–propagation phenomena*, 1st ed. Cambridge University Press, 2004.

[17] J. S. Picard and A. J. Weiss, "Time difference localization in the presence of outliers," *Signal Processing*, vol. 92, no. 10, pp. 2432–2443, Oct. 2012.

[18] W. A. Martins, L. O. Nunes, D. B. Haddad, L. W. P. Biscainho, M. V. S. Lima, M. Costa, and B. Lee, "Time-of-flight selection for improved acoustic sensor localization using multiple loudspeakers," *XXXI Simpósio Brasileiro de Telecomunicações (SBrT 2013)*, pp. 1–5, Set. 2013.

[19] J. A. Apolinário Jr., H. Yazdanpanah, A. S. Nascimento, and M. L. R. de Campos, "A Data-selective LS Solution to TDOA-based Source Localization," *IEEE International Conference on Acoustics, Speech and Signal Processing (ICASSP 2019)*, Apr. 2019.

[20] D. B. Haddad, W. A. Martins, L. W. P. Biscainho, M. V. M. Costa, and K. Kim, "Choosing coherent times of flight for improved acoustic sensor localization," *International Telecommunications Symposium (ITS 2014)*, Aug. 2014.

[21] D. B. Haddad, M. V. S. Lima, W. A. Martins, L. W. P. Biscainho, L. O. Nunes, and B. Lee, "Acoustic sensor self-localization: Models and recent results," *Wireless Acoustic Sensor Networks and Applications*, vol. 2017, Oct. 2017.

[22] D. B. Haddad, W. A. Martins, M. d. V. da Costa, L. W. Biscainho, L. O. Nunes, and B. Lee, "Robust acoustic self-localization of mobile devices," *IEEE Transactions on Mobile Computing*, vol. 15, no. 4, pp. 982–995, Aug. 2016.

[23] M. Compagnoni, A. Pini, A. Canclini, P. Bestagini, F. Antonacci, S. Tubaro, and A. Sarti, "A Geometrical–Statistical Approach to Outlier Removal for TDOA Measurements," *IEEE Transactions on Signal Processing*, vol. 65, no. 15, pp. 3960–3975, Aug. 2017.

[24] W. Xiong, C. Schindelhauer, H.So, J. Bordoy, A. Gabbrielli, and J. Liang, "TDOA–based localization with NLOS mitigation via robust model transformation and neurodynamic optimization," *Signal Processing*, vol. 178, no. 107774, pp. 1–10, Jan. 2021.

[25] I. L. Freire, P. C. Prandel, and J. A. Apolinário Jr., "Sobre a escolha de sinais em arranjos de microfones estimando DoA com GCC-PhaT - in Portuguese," *XXX Simpósio Brasileiro de Telecomunicações (SBrT 2012)*, Sep. 2012.

[26] I. L. Freire, "Robust direction-of-arrival by matched-lags, applied to gunshots," *The Journal of the Acoustical Society of America*, vol. 135, no. 6, pp. 246–251, Jun. 2014.

[27] J. G. C. Ribeiro, F. G. Serrenho, J. A. Apolinário Jr., and A. L. L. Ramos, "Improved DoA estimation with application to bearings-only acoustic source localization," in *IEEE International Symposium on Signal Proc. and Information Technology (ISSPIT 2017)*, Dec. 2017, pp. 100–105.

[28] B. Huang, L. Xie, and Z. Yang, "TDOA-based source localization with distance-dependent noises," *IEEE Transactions on Wireless Communications*, vol. 14, no. 1, pp. 468–480, Jan. 2015.

Wallace A. Martins (S'07–M'12–SM'20) received the electronics engineer degree, and the M.Sc. and D.Sc. degrees in electrical engineering from the Federal University of Rio de Janeiro (UFRJ), Rio de Janeiro, Brazil, in 2007, 2009, and 2011, respectively. He was a Research Visitor at the University of Notre Dame, USA, in 2008, Université de Lille 1, France, in 2016, and Universidad de Alcalá, Spain, in 2018. He was an Associate Professor at the Department of Electronics and Computer Engineering (DEL/Poli) and the Electrical Engineering Program (PEE/COPPE), UFRJ, from 2013 to 2022. He was Academic Coordinator and Deputy Department Chairman (DEL/Poli), UFRJ, from 2016 to 2017. He is currently a Research Scientist working with the Interdisciplinary Centre for Security, Reliability and Trust (SnT), University of Luxembourg. His research interests include digital signal processing and telecommunications, with focus on equalization and beamforming/precoding for terrestrial and non-terrestrial (satellite) wireless communications. He is a member (Associate Editor) of the Editorial Boards of the IEEE SIGNAL PROCESSING LETTERS and the EURASIP Journal on Advances in Signal Processing. He was the recipient of the Best Student Paper Award from EURASIP at EUSIPCO-2009, Glasgow, Scotland, the 2011 Best Brazilian D.Sc. Dissertation Award from Capes, and the Best Paper Award at SBrT-2020, Florianópolis, Brazil.

Daniel Patricio Nicolalde Rodríguez received a Bachelor of Science degree in Electronics and Telecommunications Engineering from Escuela Politécnica del Ejército (ESPE, Quito, Ecuador, in 2007) and a Master of Science degree in Electrical Engineer (EE) from the Military Institute of Engineering (IME, Rio de Janeiro, Brazil, in 2010). He has been working as Telecommunications Consultant, in the field of IP/MPLS and mobile networks, for companies Nokia and Huawei, and their customers since 2010. Currently, Daniel is a Ph. D. student with the Program of Electrical Engineering of the Federal University of Rio de Janeiro (UFRJ, Rio de Janeiro, Brazil). His main research areas are DSP and applications.

José Antonio Apolinário Jr. graduated from the Military Academy of Agulhas Negras (AMAN, Resende, Brazil, in 1981) and received the following degrees: B.Sc.-EE from the Military Institute of Engineering (IME, Rio de Janeiro, Brazil, in 1998), M.Sc.-EE from the University of Brasília (UnB, Brasília, Brazil, in 1993), and D.Sc.-EE from the Federal University of Rio de Janeiro (UFRJ, Rio de Janeiro, Brazil, in 1998). He is currently an Associate Professor at IME, where he has already served as Head of Department and Vice-Rector for Study and Research. He was a Visiting Professor at the Escuela Politécnica del Ejército (ESPE, Quito-Ecuador), from 1999 to 2000, and a Visiting Researcher (1997) and a Visiting Professor (2004 and 2006) at Helsinki University of Technology (now Aalto University, Espoo, Finland). His research interests comprise many aspects of DSP, including adaptive filtering, acoustics, and array processing.

Marcello L. R. de Campos was born in Niteroi, Brazil, in 1968. He received the Engineering (cum laude) degree from the Federal University of Rio de Janeiro (UFRJ), Rio de Janeiro, Brazil, in 1990, the M.Sc. degree from COPPE/UFRJ in 1991, and the Ph.D. degree from the University of Victoria, Victoria, BC, Canada, in 1995, all in Electrical Engineering. In 1996, he was Post-Doctoral Fellow with the Department of Electronics, School of Engineering, UFRJ, and with the Program of Electrical Engineering, COPPE/UFRJ. From 1997 until 1998, he was Associate Professor with the Department of Electrical Engineering, Military Institute of Engineering, Rio de Janeiro. Since 1998 he has been Professor with the Electrical Engineering Program, COPPE/UFRJ, having served as Vice-Chair and Chair in 2004 and 2005, respectively. He is currently Academic Director for COPPE, serving a four-year term ending in 2023. In 1998, he was with the Laboratory for Telecommunications Technology, Helsinki University of Technology, Espoo, Finland. In 2001, he received a Nokia Visiting Fellowship to visit the Center for Wireless Communications, University of Oulu, Oulu, Finland. In 2008, he visited Unik, the University Graduate Center of the University of Oslo, Oslo, Norway. In 2016, he visited Aalto University, Helsinki, Finland, as part of the mobility program for the Smart2 project, Erasmus Mundus Program, and in 2018 he visited the National University of Science and Technology, Norway, for a micro-sabbatical. He has taught over 150 courses on mobile communications in 15 countries. His research interests include adaptive signal processing in general and its application to distributed networks, in particular, adaptive beamforming, statistical signal processing, signal processing for communications, underwater, mobile and wireless communications, and MIMO systems. He served as the IEEE Communications Society Regional Director for Latin America in 2000 and 2001, Local-Arrangements Co-Chair for GLOBECOM99, Finance Chair for SPAWC 2008, Plenary Chair for ISCAS 2011, and Technical Co-Chair for the 2013 Brazilian Telecommunications Symposium. He founded and was Chair of the IEEE Signal Processing Society Rio de Janeiro Chapter from 2011 to 2017.